Supplementary Information

Mechanistic Insights into the Effect of Electrolyte Medium on Electrochemical Nitrogen Reduction Reaction on Copper Hexacyanoferrate Nanocubes decorated Functionalized Carbon Nanotubes

Aamir Y. Bhat[a], Priya Jain[a], Mohsin A. Bhat[c], Pravin P. Ingole[a]*

[a] *Department of Chemistry, Indian Institute of Technology Delhi, New Delhi– 110016, India*

[b] *Department of Chemistry, University of Kashmir, Hazratbal Srinagar, 190006, India*

Table S1. Summary of the representative reports on N_2 fixation at room temperature and atmospheric pressure. *NH_3 yield and F.E. are determined using indophenol blue method.

Catalysts	Electrolyte	E (V *vs.* RHE)	NH_3 yield*	F.E. s(%)*	Ref.
Fe/ Fe_3O_4	0.1 M PBS	-0.3	0.19 (μg cm^{-2} h^{-1})	8.29	[1]
FeNi PBA/rGO	0.05 M H_2SO_4	-0.2	17 (mg g^{-1} h^{-1})	27.5	[2]
CuO/RGO	0.1 M Na_2SO_4	-0.75	1.8×10^{-10} (mol cm^{-2} s^{-1})	3.9	[3]
Dentritic Cu	0.1 M HCl	-0.4	25.63 (μg mg^{-1} h^{-1})	15.12	[4]
Spinal Fe_3O_4 nanorods	0.1 M Na_2SO_4	-0.4	0.6×10^{-10} (mol cm^{-2} s^{-1})	2.6	[5]
$CoFe_2O_4$/rGO	0.1 M Na_2SO_4	-0.4	0.4×10^{-10} (mol cm^{-2} s^{-1})	6.2	[6]
Fe_2O_3/CNT	$KHCO_3$	-2	0.22 (μg $mg^{-1}h^{-1}$)	0.15	[7]
N doped porous carbon	0.05 M H_2SO_4	-	23.8 (μg mg^{-1} h^{-1})	1.4	[8]
Fe_3C@C core-shell	0.05 M H_2SO_4	-0.2	8.53 (μg mg^{-1} h^{-1})	9.15	[9]
$Fe_2(MoO_4)_3$	0.1 M Na_2SO_4	-0.7	7.5 (μg mg^{-1} h^{-1})	1.0	[10]
Ni–Fe phosphide nanoplates	0.1 M Na_2SO_4	-0.1	16.4 (μg mg^{-1} h^{-1})	39.9	[11]
Fe-doped TiO_2	0.5 M $LiClO_4$	-0.4	25.47 (μg mg^{-1} h^{-1})	25.6	[12]
CuFe PBA/f-CNT	**0.1 M KOH**	**-0.2**	**19 (μg mg^{-1} h^{-1}) 1.8×10^{-10} (mol cm^{-2} s^{-1})**	**21.8**	**This work**
	0.05 M H_2SO_4	**-0.29**	**23.94 (μg mg^{-1} h^{-1}) 2.0×10^{-10} (mol cm^{-2} s^{-1})**	**7.0**	

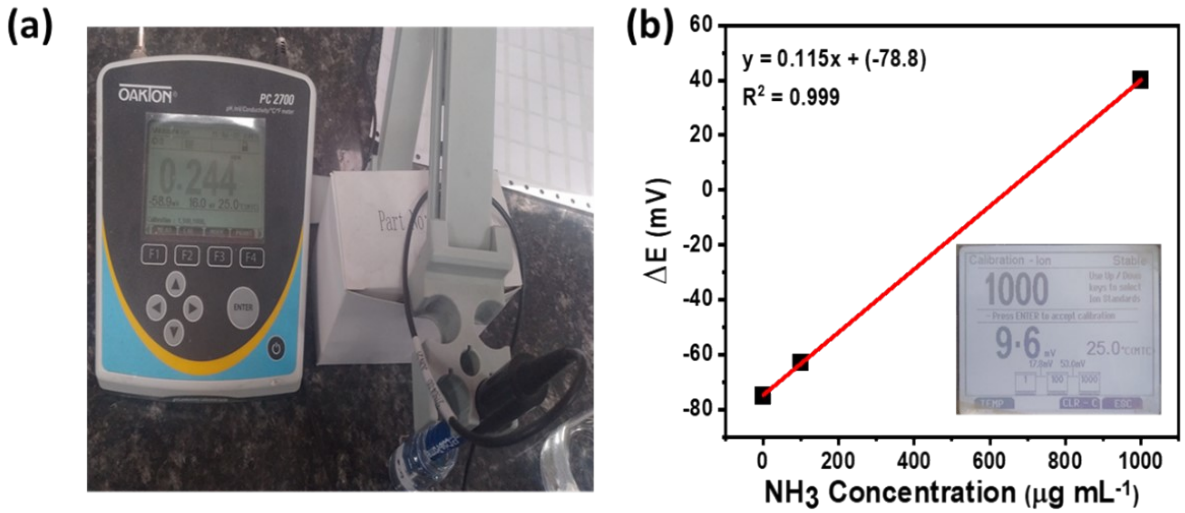

Fig. S1: (a) picture of the Ionometer used for the determination of ammonium ion concentration, (b) corresponding calibration plot.

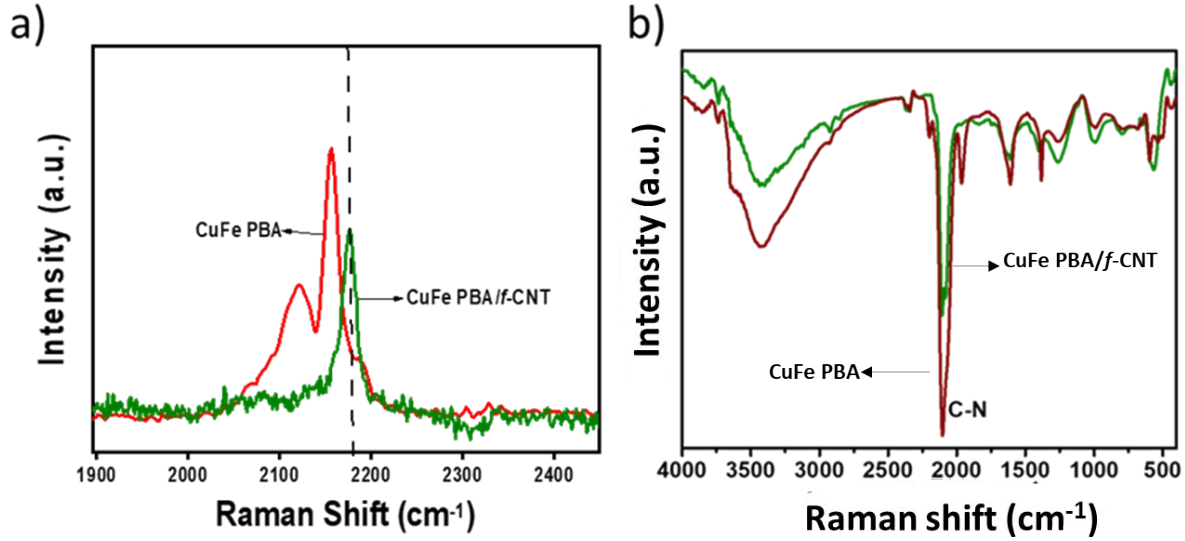

Fig. S2: Comparison of a) Raman, and b) FTIR spectra for Fe-CN-Cu band in CuFe PBA and CuFe PBA/f-CNT.

Table S2: The atomic ratio of different elements obtained from EDX analysis, intensity ratio of Cu-N-C-Fe stretching from FTIR and Raman analysis, H_2O content from TGA, intensity ratio of Fe^{3+} peak from XPS and the estimated FeCN vacancies in CuFe PBA and CuFe PBA/f-CNT.

Sample	Fe/Cu	N/Cu	C/N	H_2O %	I_{ratio} υ(CN) (FTIR)	I_{ratio} υ(CN) (Raman)	I_{ratio} Fe^{3+} (XPS)	V_{FeCN}
CuFe PBA	1.08	3.68	1.05	20.7	0.70	0.82	0.5	8 %
CuFe PBA/f-CNT	2.38	3.22	1.74	21.2				14.5 %

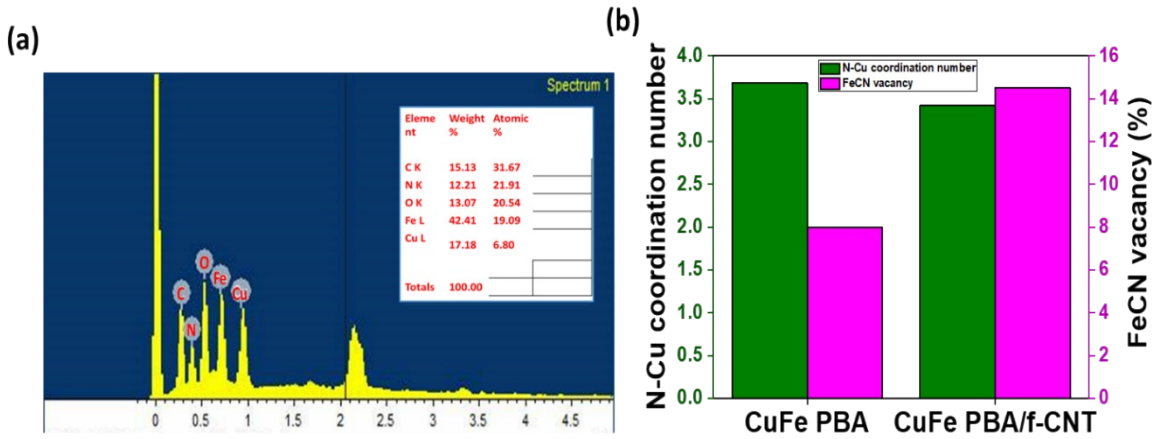

Fig. S3: (a) EDX analysis of CuFe PBA/f-MWCNT (b) The V_{FeCN} and Cu-N coordination number of CuFe PBA and CuFe PBA/f-MWCNT calculated by EDX analysis.

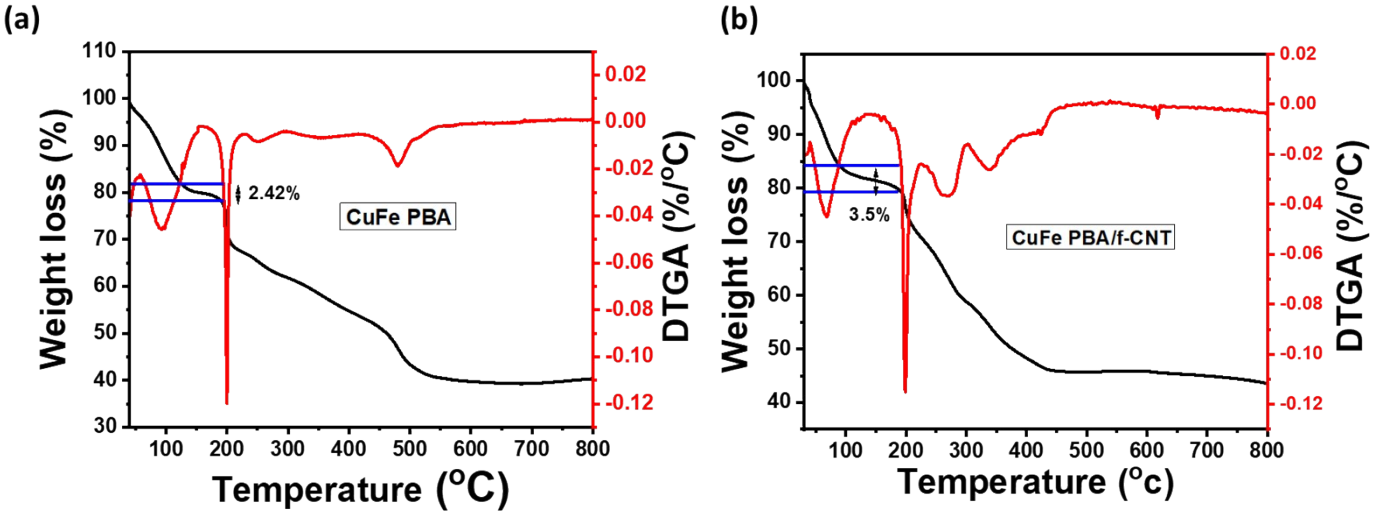

Fig. S4: TGA and DTGA curves showing the total water content (adsorbed and coordinated water) in (a) CuFe PBA and (b) CuFe PBA/f-CNT.

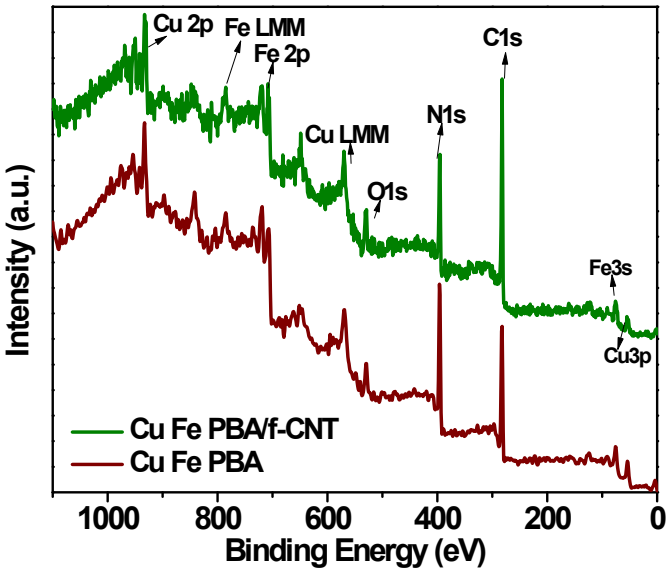

Fig. S5: XPS survey spectra of CuFe PBA and CuFe PBA/f-CNT.

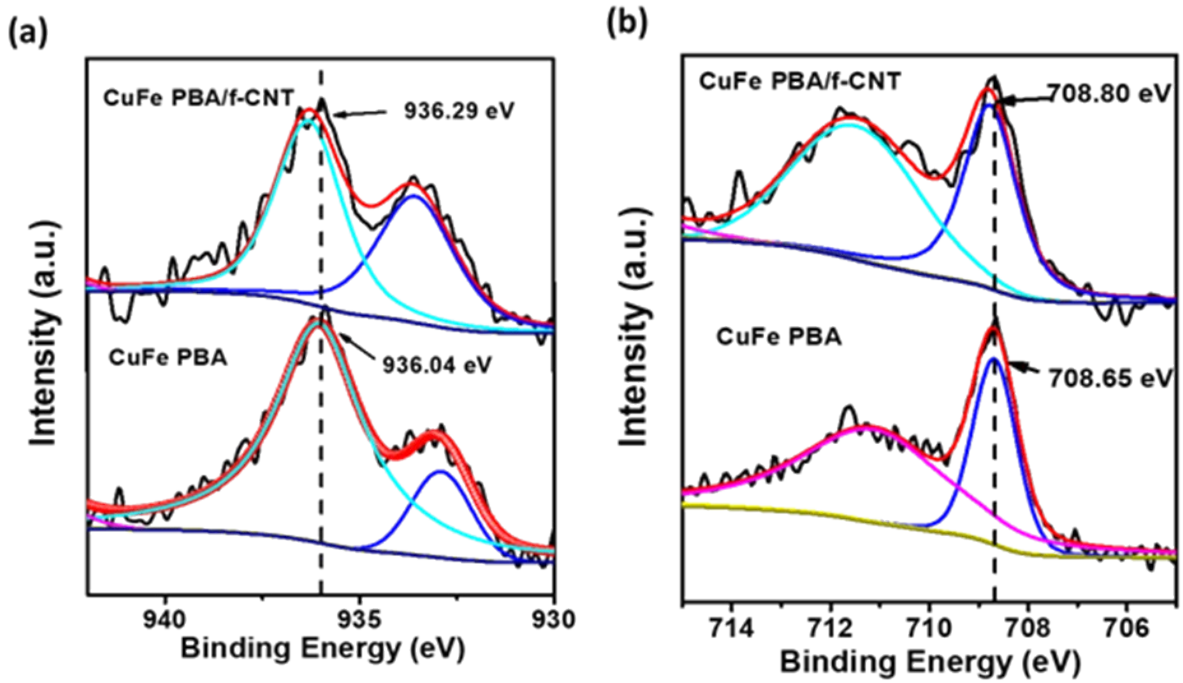

Fig. S6: Comparison of a) Cu 2p and b) Fe 2p XPS spectra of CuFe PBA and CuFe PBA/f-CNT.

Table S3: The comparison of XPS, FTIR, and Raman data for studied samples.

		CuFe PBA			**CuFe PBA/f-CNT**			
FTIR	**υ(C-N) (cm^{-1})**	Fe^{II}-CN-Cu^{I}	Fe^{II}-CN-Cu^{II}	Fe^{III}-CN-Cu^{II}	Fe^{II}-CN-Cu^{I}	Fe^{II}-CN-Cu^{II}	Fe^{III}-CN-Cu^{II}	
		2070	2103	2160	2079	2107	2161	
Raman shift	**υ(C-N) (cm^{-1})**	2154			2182			
XPS B.E.	**Cu 2p**	**Cu^{+}**	**Cu^{2+}**	**satellite**	**Cu 2p**	**Cu^{+}**	**Cu^{2+}**	**Satellite**

(eV)	**Cu $2p_{3/2}$**	932.9	936.04	944.4	$Cu2p_{3/2}$	933.5	936.3	944.0
	Cu $2p_{1/2}$	952.7	956.1	963.8	$Cu2p_{1/2}$	953.2	956.1	964.0
	Fe 2p	**Fe^{2+}**	**Fe^{3+}**	**satellite**	**Fe 2p**	**Fe^{2+}**	**Fe^{3+}**	**Satellite**
	Fe $2p_{3/2}$	708.6	711.1	715.9	$Fe2p_{3/2}$	708.7	711.4	716.2
	Fe $2p_{1/2}$	721.5	724.0	736.3	$Fe2p_{1/2}$	721.6	724.2	736.6
	N 1s	398.2			398.7			
	C 1s	**f-CNT**			**CuHCF/f-CNT**			
		C-C	**C-O**	**C=O**	**O-C=O**	**C-C**	**C-N**	**C=O**	**O-C=O**
		274.7	285.6	286.6	289.1	284.7	285.6	286.7	288.4

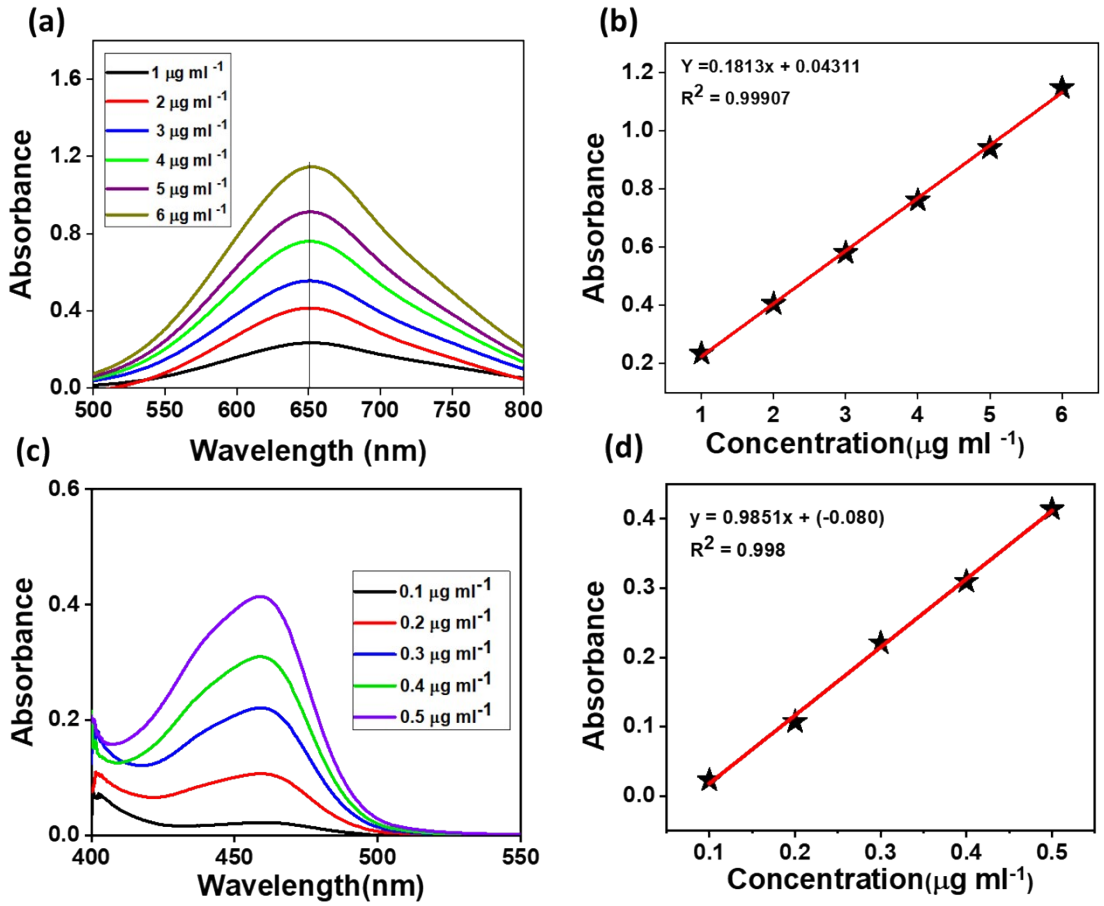

Fig. S7: (a) Absorption spectra of NH_3 with varying concentrations after 2 hrs of incubation at ambient conditions via indophenol blue method and (b) corresponding calibration curve. (c) Absorption spectra of $N_2H_4.H_2O$ with varying concentrations after 10 min. of incubation at room temperature using Watt and Chrisp method and (d) corresponding calibration curve.

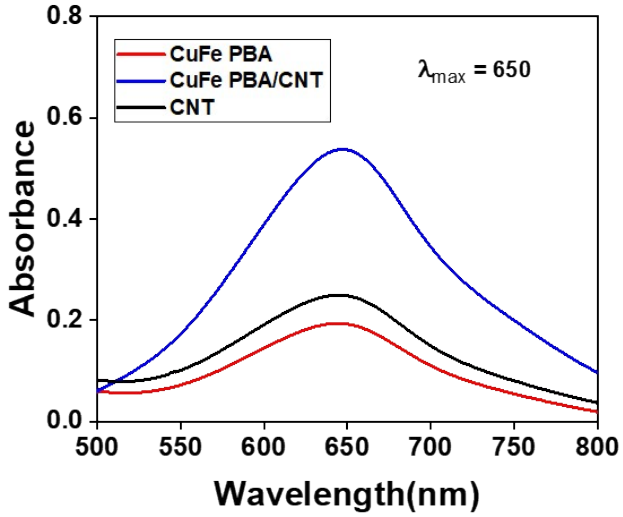

Fig. S8: Absorption spectra of electrolytes stained with indophenol blue after 2 h electrolysis of pristine CuFe PBA, CuFe PBA/*f*–CNT and *f*–CNT respectively in 0.05 M H_2SO_4.

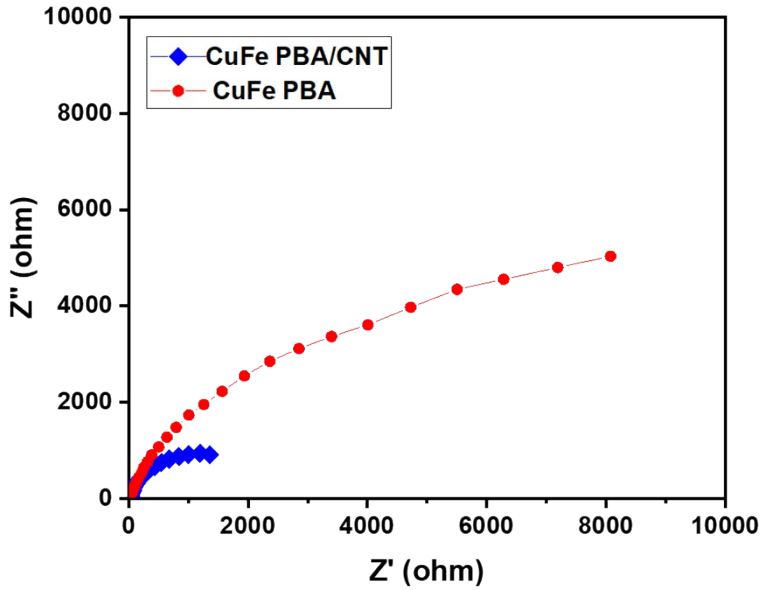

Fig. S9: (a) Nyquist plots of CuFe PBA and CuFe PBA/fCNT in 0.05 M H_2SO_4.

Determination of NO_2 contaminants:

The presence of NO_2^- in an electrolyte was estimated using N-(1-naphthyl)-ethylenediamine dihydrochloride UV–Vis spectrophotometry method[21]. For this, a colouring reagent solution was prepared by mixing of 5 mL of acetic acid, 5 mg of N-(1-naphthyl)-ethylenediamine dihydrochloride, and 0.5 g of sulfanilic acid in 95 mL of water. Then to 1 mL of electrolyte, 4 mL of colouring solution was added and absorption at 550 nm was measured after incubating the mixture for 15 minutes at room temperature. (Inset Fig. S10a in the revised SI). Prior to that, standard solutions with varying concentrations of NO_2^- ($NaNO_2$) were prepared and the absorption at 550 nm was measured after the 15 min of incubation. A good linear relation was observed between absorbance and concentration (Fig. S10a & b).

Determination of NO_3 contaminants: The presence of any possible nitrate (NO_3^-) contamination was identified through UV visible spectroscopy. Briefly, 0.1 mL of 1 M HCl was added to 5 mL of electrolyte and absorption was measured at 220 nm after incubating the mixture for 10 minutes. A calibration plot for determining the concentration of NO_3 was also plotted using standard solutions of $NaNO_3$ with varying concentrations (1-5ppm) (Fig. S10c&d)

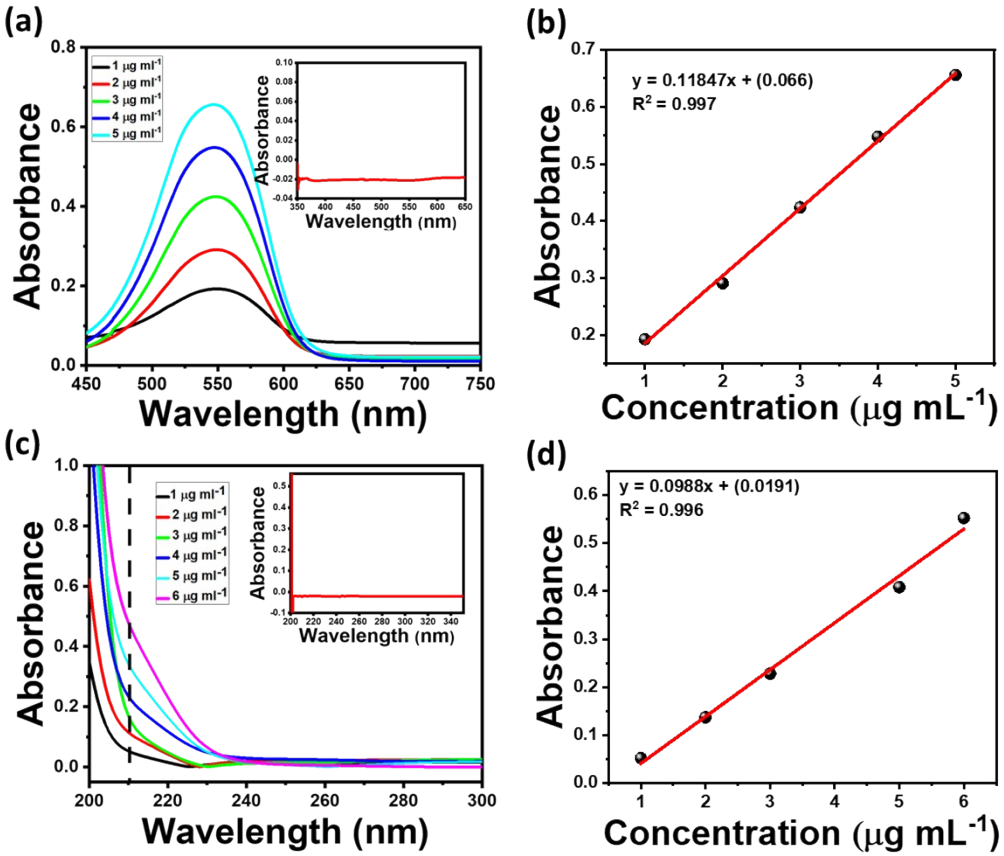

Fig. S10: (a) UV absorption spectra of different standard concentrations of $NaNO_2$ and electrolyte (inset), (b) corresponding calibration plot, (c) UV absorption spectra of various standard concentrations of $NaNO_3$ and electrolyte (inset), (d) corresponding calibration plot.

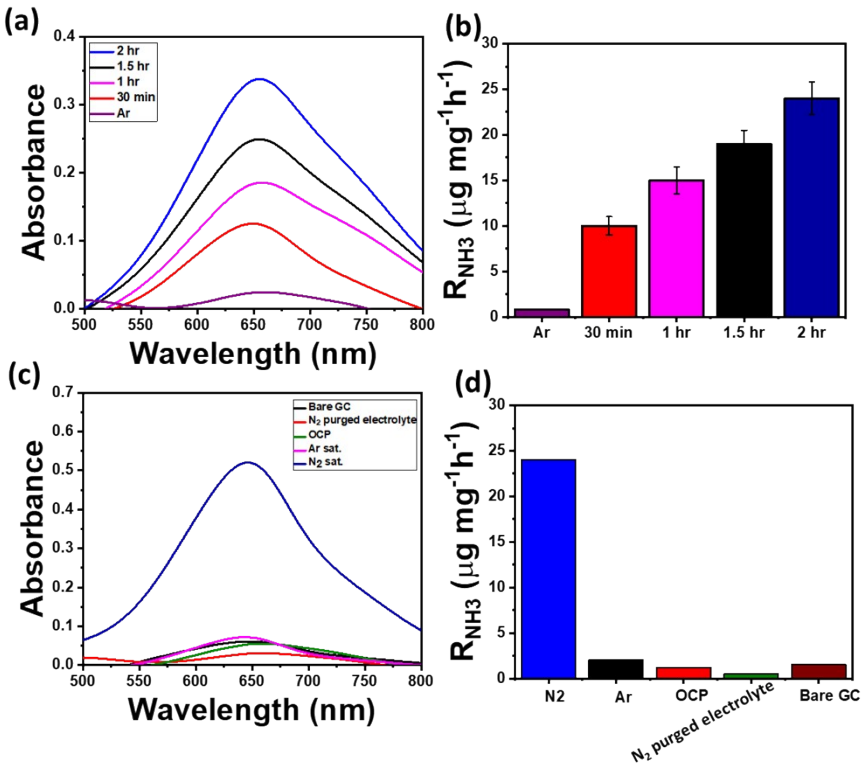

Fig.S11: (a) UV absorption spectra of electrolyte after different time intervals using indophenol blue method, (b) corresponding NH_3 yield rate, (c) UV absorption spectra of electrolyte under various conditions and (d) corresponding NH_3 yield.

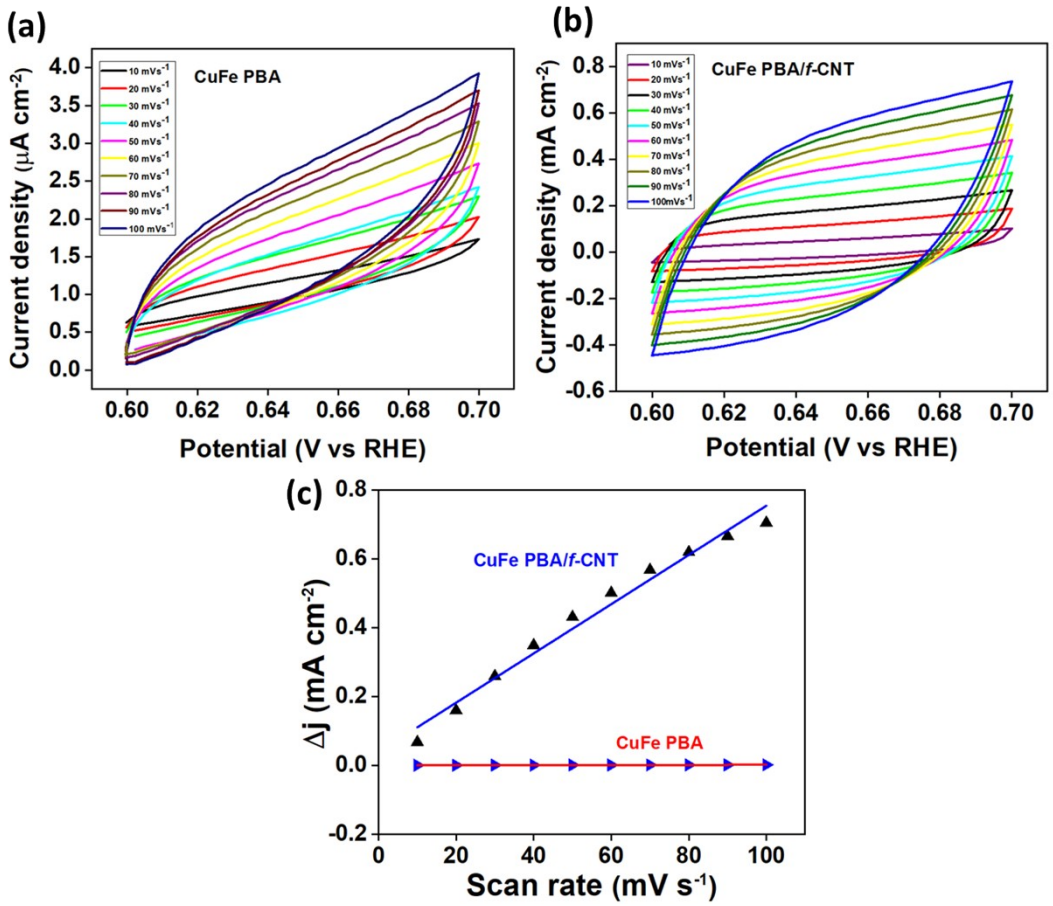

Fig S12: Cyclovoltagram for (a) pristine CuFe PBA, (b) CuFe PBA/f-CNT, (c) charge current density about difference Δj plotted against scan rate.

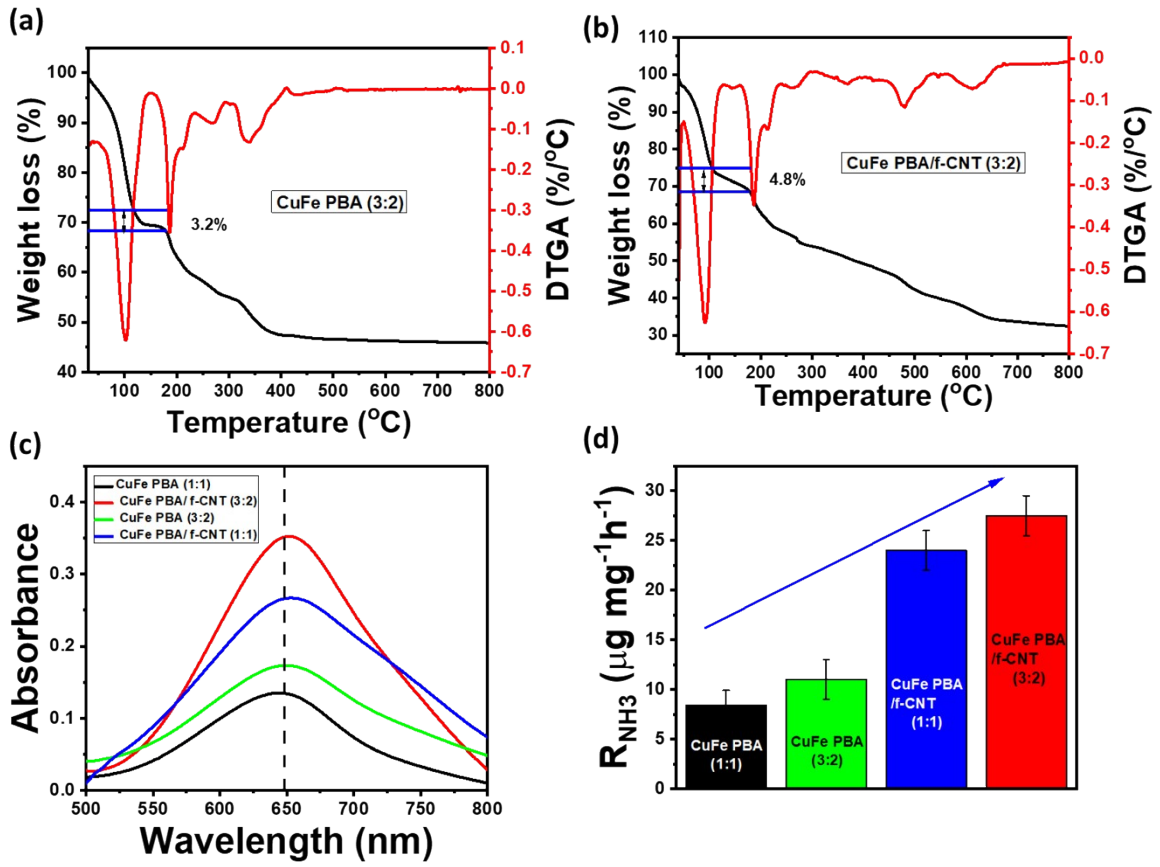

Fig. S13: TGA and DTGA curves showing the total water content (adsorbed and coordinated water) in (a) CuFe PBA (3:2) and (b) CuFe PBA /f-CNT (3:2), (c) The comparison of UV absorption spectra (indophenol blue method) for CuFe PBA (1:1), CuFe PBA (3:2), CuFe PBA/f-CNT (1:1) and CuFe PBA/f-CNT (3:2) in 0.05 M H_2SO_4 at -0.29 V vs RHE. (d) Corresponding NH_3 yield rate.

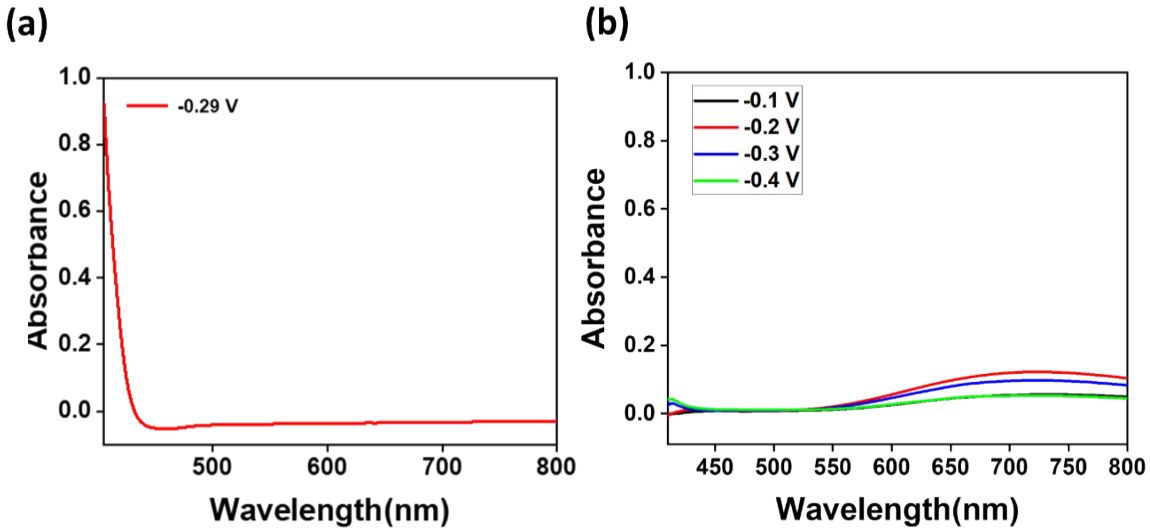

Fig. S14: UV absorption spectra of electrolyte after 2 h electrolysis estimated by the method of Watt and Chrisp, (a) in 0.5 M H_2SO_4, (b) in 0.1 M KOH.

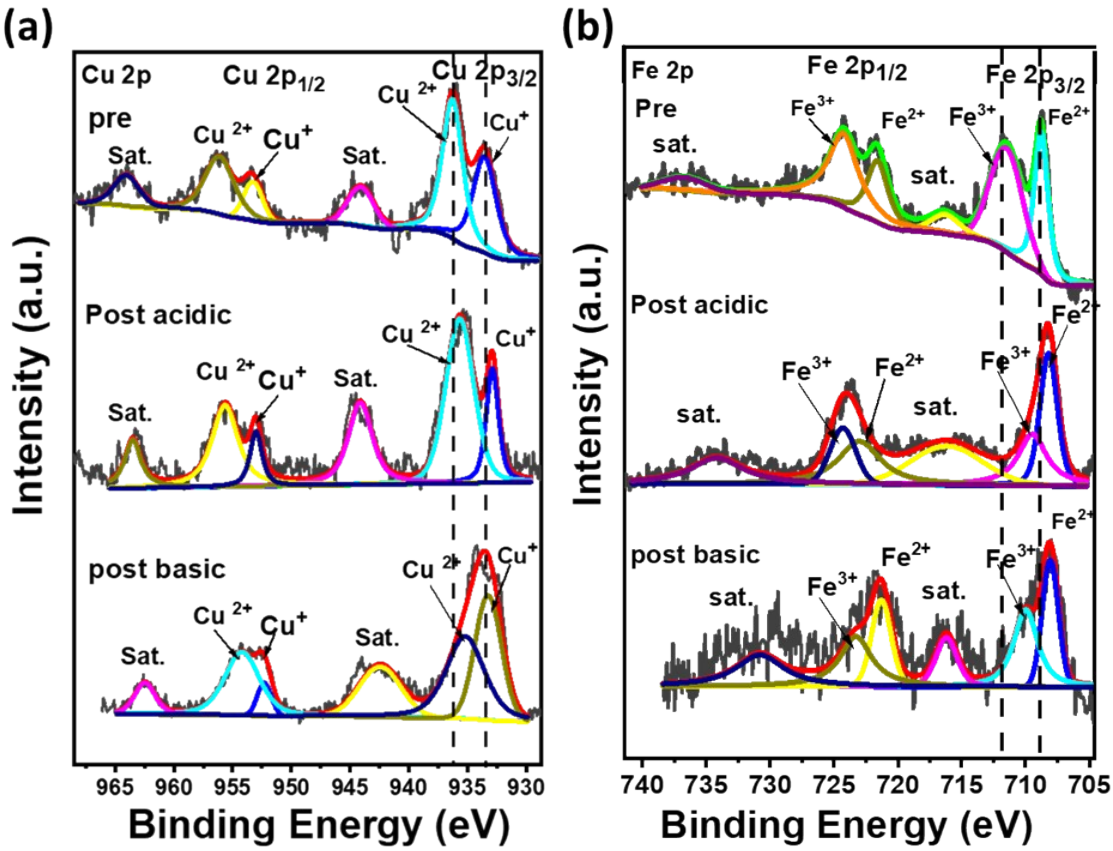

Fig. S15: XPS spectra of (a) Cu 2p and (b) Fe 2p before and after stability test in 0.05 M H_2SO_4. and 0.1 M KOH.

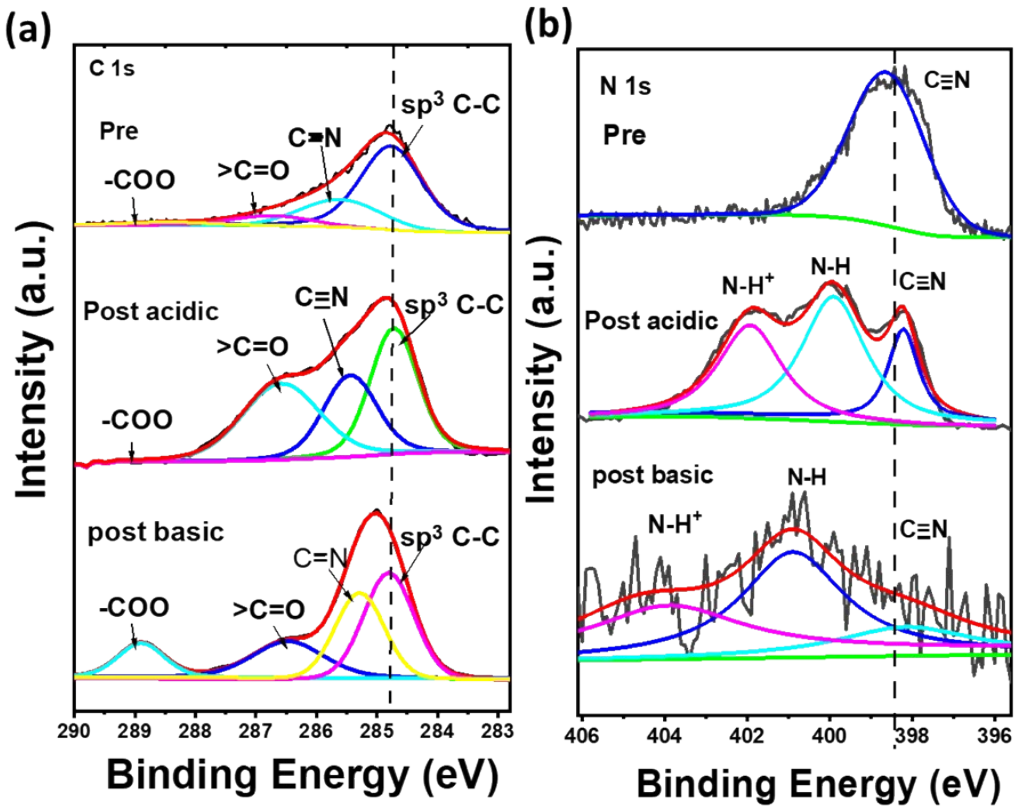

Fig. S16: XPS spectra of (a) C 1s and (b) N 1s before and after stability test in 0.05 M H_2SO_4 and 0.1 M KOH.

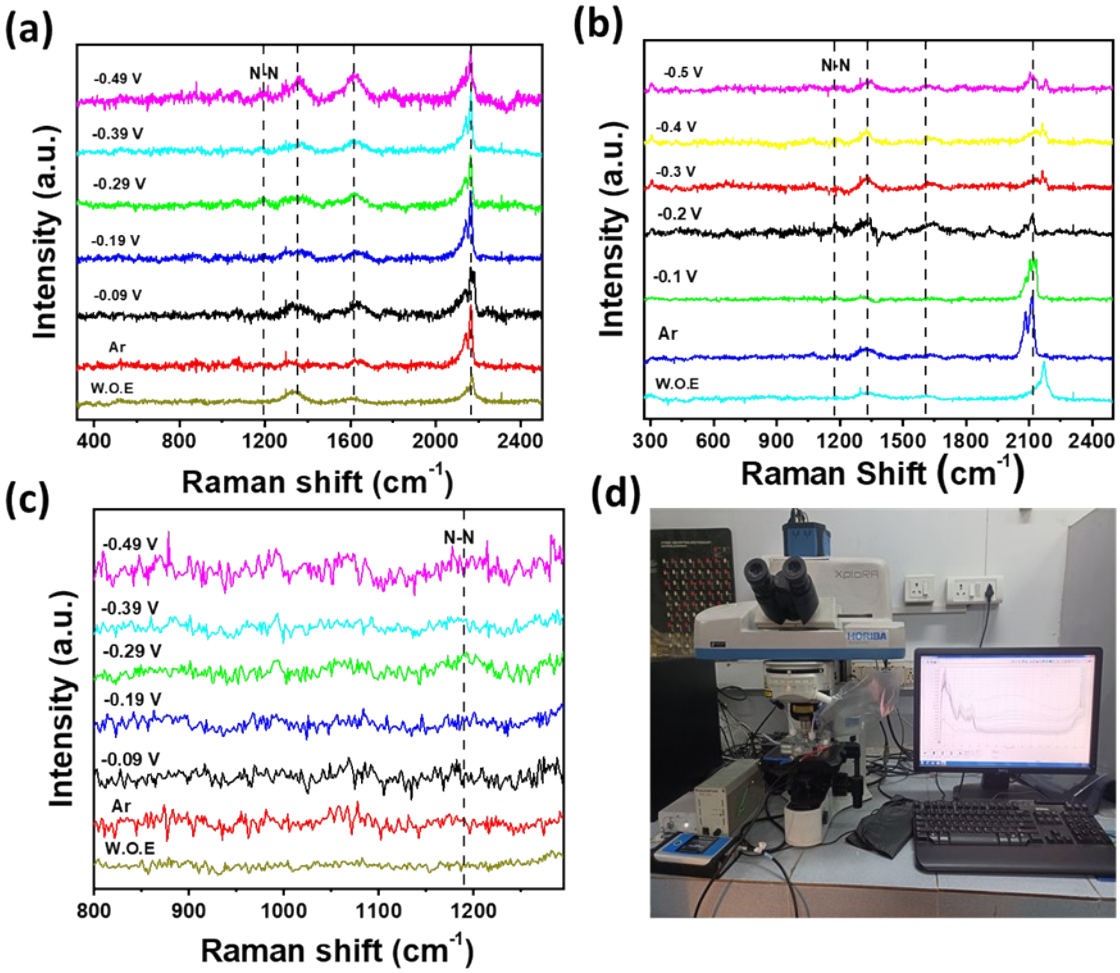

Fig. S17: In-situ Raman analysis in (a) 0.05 M H_2SO_4, (b) 0.1 M KOH solution, (c) zoomed portion of in-situ Raman spectra, (d) image of the Raman instrument used for in-situ Raman analysis.

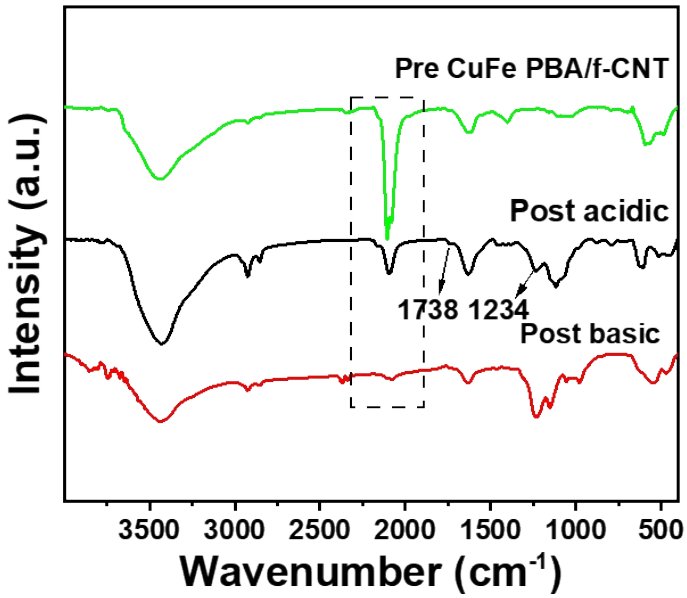

Fig. S18: Ex-situ FTIR analysis before and after electrolysis in 0.05 M H_2SO_4 and 0.1 M KOH.

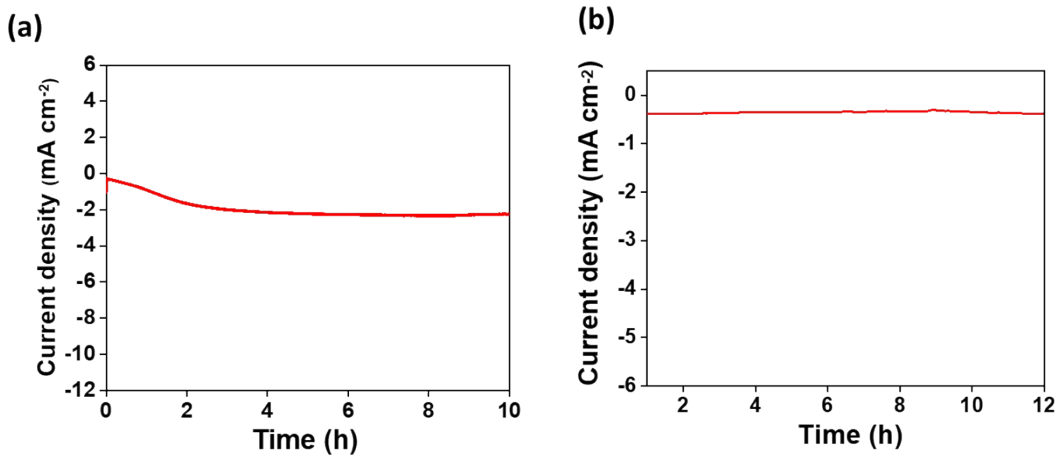

Fig. S19: (a) Chronoamperometry for 10 hr at -0.29 V vs RHE in 0.05 M H_2SO_4. (b) Chronoamperometry for 12 hours at -0.2 V vs RHE in 0.1 M KOH.

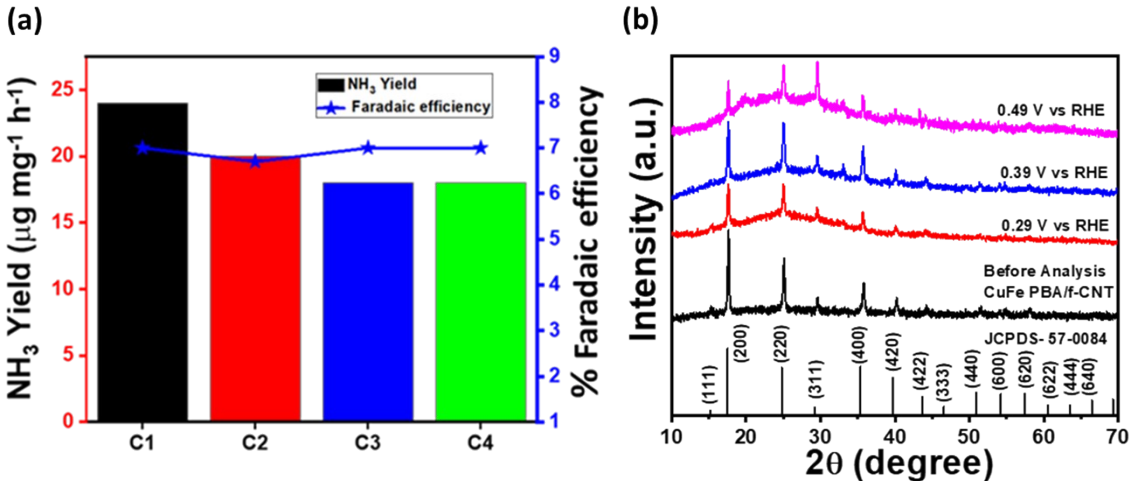

Fig. S20: (a) Recycling test of CuFe PBA/*f*-CNT for ENRR in acidic medium at the potential of -0.29V vs RHE. (b) XRD pattern of CuFe PBA/*f*-CNT after chronoamperometric evaluation at different potentials.

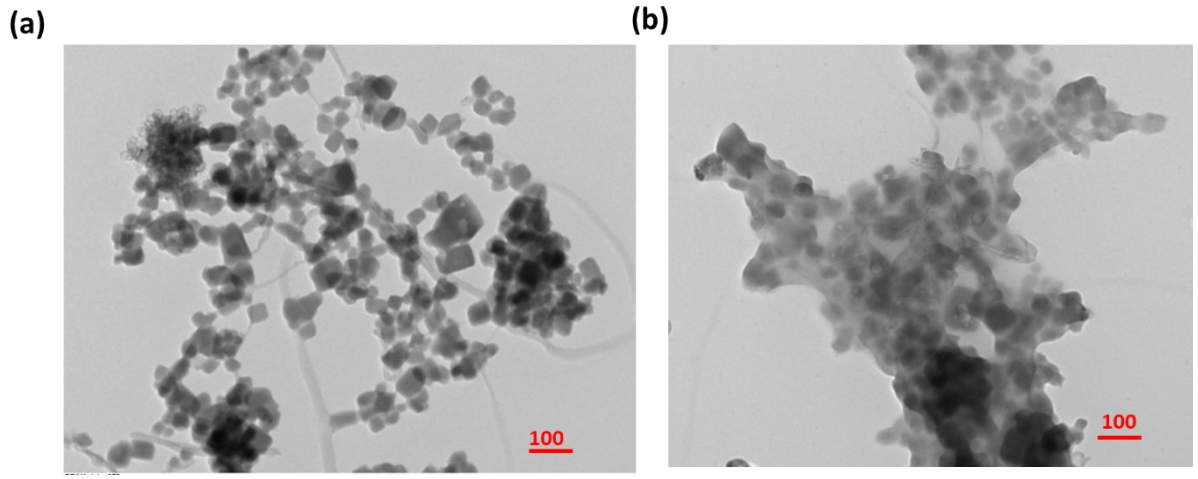

Fig. S21: TEM images of CuFe PBA/*f*-CNT (a) before and (b) after stability test in 0.05 M H_2SO_4.

References:

(1) Hu, L.; Khaniya, A.; Wang, J.; Chen, G.; Kaden, W. E.; Feng, X. Ambient Electrochemical Ammonia Synthesis with High Selectivity on Fe/Fe Oxide Catalyst. *ACS Catal.***2018**, *8* (10), 9312–9319. https://doi.org/10.1021/ACSCATAL.8B02585/SUPPL_FILE/CS8B02585_SI_001.PDF .

(2) Tao, T.; Wang, J.; Xu, M.; Fang, Z.; Li, W. Ultrasmall Size FeNi Prussian Blue Analogue on RGO with Accurate Heteronuclear Adsorption Sites toward Efficient Electrochemical Nitrogen Fixation. *Int. J. Hydrogen Energy* **2021**, *46* (21), 11731–11739. https://doi.org/10.1016/j.ijhydene.2021.01.091.

(3) Wang, F.; Liu, Y.; Zhang, H.; Chu, K.; Wang, F.; Liu, Y.; Chu, K.; Zhang, H. CuO/Graphene Nanocomposite for Nitrogen Reduction Reaction. *ChemCatChem* **2019**, *11* (5), 1441–1447. https://doi.org/10.1002/CCTC.201900041.

(4) Li, C.; Mou, S.; Zhu, X.; Wang, F.; Wang, Y.; Qiao, Y.; Shi, X.; Luo, Y.; Zheng, B.; Li, Q.; Sun, X. Dendritic Cu: A High-Efficiency Electrocatalyst for N_2 Fixation to NH_3 under Ambient Conditions. *Chem. Commun.* **2019**, *55* (96), 14474–14477. https://doi.org/10.1039/c9cc08234d.

(5) Liu, Q.; Zhang, X.; Zhang, B.; Luo, Y.; Cui, G.; Xie, F.; Sun, X. Ambient N_2 Fixation to NH_3 Electrocatalyzed by a Spinel Fe_3O_4 Nanorod. *Nanoscale* **2018**, *10* (30), 14386–14389. https://doi.org/10.1039/C8NR04524K.

(6) Ahmed, M. I.; Chen, S.; Ren, W.; Chen, X.; Zhao, C. Synergistic Bimetallic $CoFe_2O_4$ Clusters Supported on Graphene for Ambient Electrocatalytic Reduction of Nitrogen to Ammonia. *Chem. Commun.* **2019**, *55* (81), 12184–12187. https://doi.org/10.1039/C9CC05684J.

(7) Chen, S.; Perathoner, S.; Ampelli, C.; Mebrahtu, C.; Su, D.; Centi, G. Electrocatalytic Synthesis of Ammonia at Room Temperature and Atmospheric Pressure from Water and Nitrogen on a Carbon-Nanotube-Based Electrocatalyst. *Angew. Chemie* **2017**, *129* (10), 2743–2747. https://doi.org/10.1002/ANGE.201609533.

(8) Liu, Y.; Su, Y.; Quan, X.; Fan, X.; Chen, S.; Yu, H.; Zhao, H.; Zhang, Y.; Zhao, J. Facile Ammonia Synthesis from Electrocatalytic N_2 Reduction under Ambient Conditions on N-Doped Porous Carbon. *ACS Catal.* **2018**, *8* (2), 1186–1191. https://doi.org/10.1021/ACSCATAL.7B02165/SUPPL_FILE/CS7B02165_SI_001.PDF .

(9) Peng, M.; Qiao, Y.; Luo, M.; Wang, M.; Chu, S.; Zhao, Y.; Liu, P.; Liu, J.; Tan, Y. Bioinspired Fe_3C@C as Highly Efficient Electrocatalyst for Nitrogen Reduction Reaction under Ambient Conditions. *ACS Appl. Mater. Interfaces* **2019**, *11* (43), 40062–40068. https://doi.org/10.1021/ACSAMI.9B14143/SUPPL_FILE/AM9B14143_SI_001.PDF.

(10) Chen, C.; Liu, Y.; Yao, Y. Ammonia Synthesis via Electrochemical Nitrogen Reduction Reaction on Iron Molybdate under Ambient Conditions. *Eur. J. Inorg. Chem.* **2020**, *2020* (34), 3236–3241. https://doi.org/10.1002/EJIC.202000554.

(11) Jiang, X.; He, M.; Tang, M.; Zheng, Q.; Xu, C.; Lin, D. Nanostructured Bimetallic Ni–Fe Phosphide Nanoplates as an Electrocatalyst for Efficient N_2 Fixation under Ambient Conditions. *J. Mater. Sci.* **2020**, *55* (31), 15252–15262. https://doi.org/10.1007/S10853-020-05085-5.

(12) Wu, T.; Iaojuan Zhu, X.; Xing, Z.; Hiyong Mou, S.; Li, C.; Qiao, Y.; Liu, Q.; Luo, Y.; Shi, X.; Zhang, Y.; Sun, X. Greatly Improving Electrochemical N_2 Reduction over TiO_2 Nanoparticles by Iron Doping. *Angew. Chemie Int. Ed.* **2019**, *58* (51), 18449–18453. https://doi.org/10.1002/ANIE.201911153.